Influence of Framework Al Density in Chabazite Zeolites on Copper Ion Mobility and Reactivity During NO_x Selective Catalytic Reduction with NH_3

Siddarth H. Krishna[1], Anshuman Goswami[2], Yujia Wang[3], Casey B. Jones[1], David P. Dean[1], Jeffrey T. Miller[1], William F. Schneider[2], Rajamani Gounder[1,*]

[1]*Charles D. Davidson School of Chemical Engineering, Purdue University, 480 Stadium Mall Drive, West Lafayette, IN 47907, USA*

[2]*Department of Chemical and Biomolecular Engineering, University of Notre Dame, Notre Dame, IN 46556, USA*

[3]*Department of Chemistry and Biochemistry, University of Notre Dame, Notre Dame, IN 46556, USA*

*Corresponding author: rgounder@purdue.edu

Abstract

Cu-zeolites catalyze low-temperature (<523 K) selective catalytic reduction (SCR) of nitrogen oxides (NO_x) via a Cu^I/Cu^{II} redox cycle involving NH_3-solvated mononuclear Cu^I and binuclear Cu^{II} complexes. Cationic Cu complexes are ionically tethered to anionic charges at Al sites in zeolite lattices, conferring mobility that allows mononuclear and binuclear Cu complexes to dynamically interconvert during SCR. Cu^I oxidation requires pairing of two $Cu^I(NH_3)_2$ complexes to react with O_2 to form binuclear intermediates, implying that Cu^I oxidation kinetics should depend on the density of framework Al centers. Here, we combine statistical simulations, steady-state kinetic measurements, and *operando* and transient X-ray absorption spectroscopy to interrogate Cu-chabazite (Cu-CHA) zeolites of varying framework Al density (0.2–1.7 Al per *cha* cage). Increasing Al density leads to systematic increases in both the fraction of Cu^I ions that are SCR-active (i.e., O_2-oxidizable) and Cu^I oxidation rate constants (per Cu), revealing new insights into how anionic Al centers in zeolite frameworks regulate the mobility of ionically tethered Cu cations and their dynamic reactivity during low-temperature NO_x SCR.

Table of Contents Image

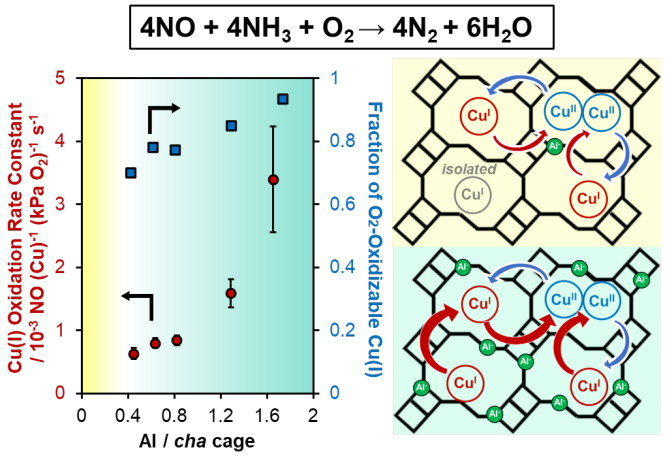

1. Introduction

The structure and reactivity of heterogeneous catalysts are conventionally described by models of active sites that treat them as static and non-interacting entities during catalytic reactions.[1–3] Yet, a growing body of literature has identified heterogeneous catalysts that exhibit dynamic behavior[4–11] wherein active sites restructure in response to changes in their reaction environment or even during steady-state catalytic turnover. Such systems sometimes display kinetic behavior that is not well-described by mean-field models, but rather non-mean-field behavior that depends on the proximity and mobility of active sites.[4] An exemplar case is that of isolated and low-nuclearity cationic metal sites supported on zeolite frameworks,[12] which are microporous, crystalline and electrically insulating silica-based lattices that can host localized anionic charges upon Al substitution for Si. Small molecules (e.g., H_2O, NH_3) can solvate associated metal ions to form mobilized and ionically tethered molecular complexes, enabling dynamic interconversion between different active site structures during catalysis.[5,6,13–20]

The selective catalytic reduction (SCR) of NO_x with NH_3 using Cu-exchanged zeolites is an example wherein kinetic and spectral data have unambiguously revealed non-mean-field kinetic behavior. [4,5,21] The small-pore chabazite (CHA) topology is used in commercial NO_x-SCR diesel aftertreatment catalysts.[22,23] The majority of diesel NO_x emissions occur at low exhaust temperatures (<523 K),[24,25] motivating interrogation of the mechanism and active site requirements under these conditions.[26] The "standard" SCR reaction (involving O_2 as the oxidant; Eqn. 1) occurs via a redox cycle in which NO and NH_3 reduce Cu^{II} to Cu^{I}, and O_2 re-oxidizes Cu^{I} to Cu^{II}.[16,27–30]

$$4NO + 4NH_3 + O_2 \rightarrow 4N_2 + 6H_2O \qquad (Eqn.\ 1)$$

NH_3 solvates and mobilizes Cu cations (<523 K), which remain ionically tethered to charge-balancing framework Al.[5,13,15–17,31–33] NH_3-solvated Cu ions pair and react with O_2 to form binuclear Cu^{II} complexes in the oxidation half-cycle, facilitated by the mobility of the $Cu^{I}(NH_3)_2$ complexes within the *cha* cages and their ability to traverse 8-membered ring (8-MR) windows into adjacent cages.[5] Mononuclear Cu^{I} and binuclear Cu^{II} sites thus dynamically interconvert during steady-state NO_x-SCR,[5,34] reminiscent of mechanisms of O_2-assisted oxidation of Cu^{I} sites via multinuclear intermediates in homogeneous and bio-inorganic catalysts.[35–38] Such dynamic behavior leads to steady-state SCR rates that show a nearly dual-site dependence on Cu density[5,39,40] in the Cu^{I}-oxidation-limited regime wherein $Cu^{I}(NH_3)_2$ is the most abundant reactive intermediate (MARI).[5] Spatial or functional isolation of a fraction of Cu^{I} sites leaves them unable to react with O_2.[5,41]

Such non-mean-field behavior implies that SCR rates are sensitive to zeolite compositional and structural properties that affect the proximity and mobility of Cu cation sites,[4] such as the density and arrangement of framework Al anionic charges. Scheme 1 depicts a two-dimensional representation of the CHA lattice in which each node represents a tetrahedral site and the hexagonal network captures the simultaneous membership of every node in three cages, with various arrangements of two Al centers charge-compensated by Cu^{I} sites depicted to show Cu ion pairing when Cu are separated by different numbers of *cha* cages via 8-MR windows. $Cu^{I}(NH_3)_2$ can migrate to access "local" cages (depicted by green circles in Scheme 1). Density functional theory (DFT) calculations predict this migration (Scheme 1a) to occur with free energy barriers as low as 20 kJ mol^{-1} (423 K) if the destination cage is vacant and ~35 kJ mol^{-1} when the destination cage is occupied with another ion, including a second $Cu^{I}(NH_3)_2$.[5,42] $Cu^{I}(NH_3)_2$ migration into *cha* cages remote to the charge-balancing Al center (Scheme 1b) are

reported to have higher free energy barriers of 60-80 kJ mol^{-1} (473 K), according to *ab initio* molecular dynamics (AIMD).[5,42] These results collectively indicate that $Cu^{I}(NH_3)_2$ can readily access the three *cha* cages shared by an Al center through local migrations, and more remote cages at a higher free energy cost. Calculations by various authors have shown that O_2 activation is facile at co-caged Cu^{I} sites, suggesting O_2 activation is kinetically irrelevant relative to Cu^{I} ion migration to co-localize in the same *cha* cage.[5,43,44]

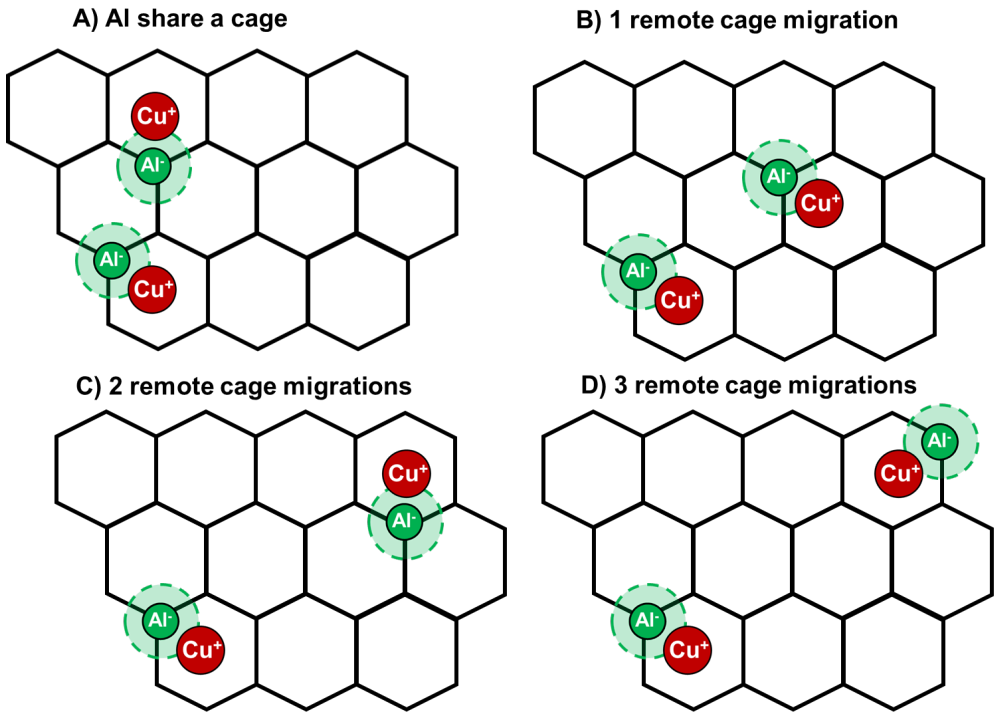

Scheme 1. Schematic representation of pairing of Cu^{I} cations ionically tethered to framework Al, when separated by "n" remote *cha* cages (A: n = 0; B: n = 1; C: n = 2; D: n = 3). The *cha* lattice represented two-dimensionally as a hexagonal lattice with faces representing *cha* 8-MR, given that each *cha* cage is connected to three other *cha* cages via 8-MR.

Experimental evidence shows that SCR kinetics depend on zeolite composition. Gao et al. observed that SCR rates (398–443 K) increase with Al density in CHA (Si/Al = 35, 12, 6; 0.5–1.0 wt% Cu), which was attributed to rate promotion by Brønsted acid sites.[45] Godiksen et al. inferred that Cu sites exchanged at CHA 6-MR (Al-O-Si-O-Al) sites oxidize faster than those

at (Al-O-Si-O-Si-O-Al) sites based on transient O_2-assisted oxidation observed by *in situ* electron paramagnetic resonance (EPR) spectroscopy.[46] Lee et al. reported that NH_3-solvated $Cu^{II}OH$ ions are more mobile and reactive than NH_3-solvated Cu^{II} ions (423-523 K, 0.05 kPa NO, 0.05 kPa NH_3, 10 kPa O_2) under conditions in which Cu ion mobility was proposed to be kinetically relevant (e.g., lower Cu densities and conditions without co-fed H_2O), based on materials progressively hydrothermally aged to vary Cu speciation[47] or Co^{2+}-pre-titrated to remove Cu^{II} sites.[48] All these conclusions were based on measured apparent rates at fixed reactant pressures, which convolve the kinetics of Cu^{I} oxidation and Cu^{II} reduction half-cycles. However, the kinetics of these two half-cycles depend differently on zeolite structural properties due to their different mechanistic and active site requirements. Thus, the underlying influence of framework Al anionic charges on the mobility and reactivity of NH_3-solvated Cu cation sites during the NO_x-SCR redox cycle remains unclear.

The single crystallographically distinct tetrahedral site, and availability of synthetic methods to vary the density and arrangement of framework Al, make CHA zeolites ideal materials for relating dynamic catalytic behavior to material composition.[15,49–52] The kinetics of Cu^{I} oxidation and Cu^{II} reduction half-cycles[5,53–55] can be isolated by varying the O_2 pressure during steady-state NO_x-SCR.[53] Here, we employ that strategy to collect kinetic and spectroscopic information over Cu-CHA zeolites of widely varying Al density to quantify the dependence of each half-cycle on macroscopic compositional parameters, and use statistical analysis to relate those observations to microscopic Cu and Al spatial distribution features. The results reveal that anionic Al centers in zeolite frameworks are not simply a host for cationic Cu complexes, but regulate the mobility of ionically tethered Cu cations and their reactivity during low-temperature NO_x SCR, and more strongly for the Cu^{I} oxidation half-cycle.

2. Results and Discussion

2.1. Steady-state Kinetics and *Operando* XAS on Cu-CHA Zeolites of Varying Cu and Al Density

To investigate the convolved effects of Cu and Al density on NO_x-SCR reactivity, Cu-CHA materials were synthesized with widely varying Al density (Table S1, SI) by adapting reported procedures including hydrothermal synthesis from molecular precursors (0.2–1.3 Al per double six-membered ring building unit, or *d6r*, corresponding to Si/Al ratios of 8–52)[15,49–52] and FAU-to-CHA interconversion (1.7 Al/*d6r*, corresponding to an Si/Al ratio of 6);[29] additional details provided in Section S1.1, SI. Cu was then introduced via aqueous $Cu(NO_3)_2$ ion-exchange to prepare a suite of materials with widely varying Al and Cu densities (0.06–0.27 Cu/*d6r*); additional details provided in Section S1.2, SI. The values reported for Al and Cu per *d6r* are bulk compositional parameters; because each *d6r* contains 12 T-sites, normalization by *d6r* or by the number of 12-T-site *cha* cages is equivalent. To aid in understanding how changes in Cu-CHA bulk material composition influence the spatial distribution of various active site ensembles, we performed statistical calculations to estimate the proximity of framework Al, extraframework Cu, and various Cu and NH_4^+ multi-site ensembles as a function of bulk Cu and Al density; additional details provided in Section S2, SI.

Figure 1a-c displays SCR rates (per total Cu) as a function of O_2 pressure on Cu-CHA zeolites of similar Cu density but varying Al density (data presented on a log-log scale in Figure S12, SI). SCR rates on all samples display a Langmuirian dependence on O_2 pressure; increasing O_2 pressures leads to a gradual transition from Cu^I oxidation (first-order in O_2) to Cu^{II} reduction (zero-order in O_2) as the dominant kinetically relevant step.[53] SCR rates (per Cu) are generally

lower at lower Cu densities (Figure 1a) than at higher Cu densities (Figure 1b, 1c), consistent with prior data.[53] When comparing samples at a given Cu density (Figures 1a-c), SCR rates in the low-O_2 pressure limit (<10 kPa O_2) increase with Al density, particularly at the highest Al densities studied (>1 Al/*d6r*). In contrast, SCR rates at higher O_2 pressures (>10 kPa O_2) show a non-monotonic dependence on Al density, with maximal rates at intermediate Al densities (0.8 Al/*d6r*).

To assess whether reactivity differences as a function of Cu-CHA composition reflect differences in *ex situ* speciation of mononuclear Cu^{II} sites, we synthesized Cu-CHA zeolites at similar bulk Cu (~0.21 Cu/*d6r*) and Al (0.8 Al/*d6r*) density but varying fractions of 6-MR paired Al sites to vary the fraction of Cu^{II} and $Cu^{II}OH$ sites.[51,52] Such materials showed indistinguishable kinetic behavior (Figure 1d), demonstrating that *ex-situ* mononuclear Cu ion speciation does not influence low-temperature SCR kinetics (additional discussion in Section S5.1, SI). Consistent with prior work,[53,56–58] we observe a fractional negative reaction order (-0.2 to -0.7) with respect to NH_3. As shown in Table S4, such NH_3 inhibition effects display no systematic trend as a function of O_2 pressure or Cu-CHA sample composition. These results suggest that NH_3 inhibition effects are not associated with only one kinetic regime, and do not depend strongly on Cu or Al density.

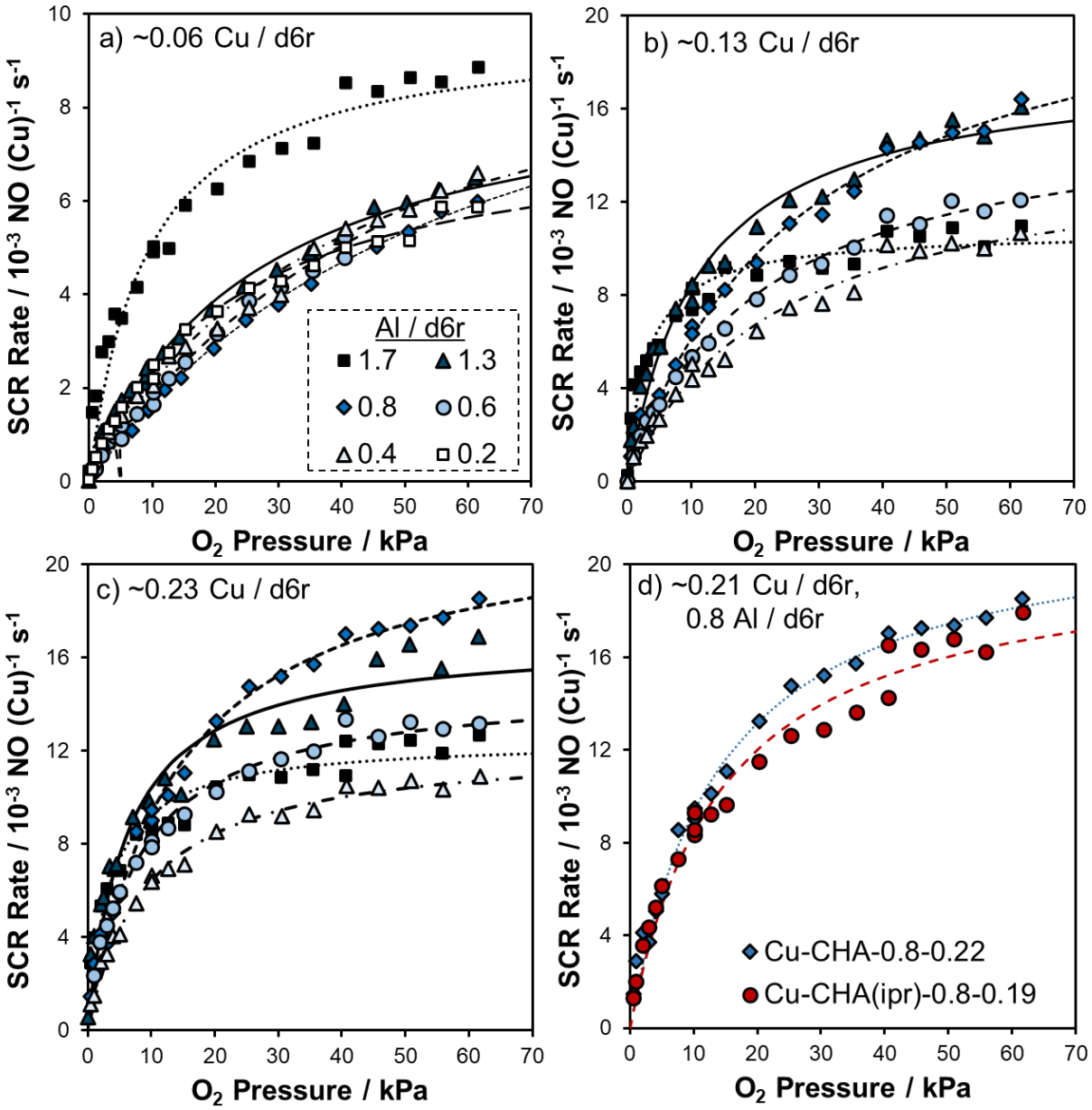

Figure 1. SCR rates (per Cu) as a function of O_2 pressure, on Cu-CHA samples of varying Al density, at various Cu densities: a) ~0.06 Cu/*d6r*, b) ~0.13 Cu/*d6r*, or c) ~0.23 Cu/*d6r*; d) at fixed Cu density (~0.21 Cu/*d6r*) and Al density (0.8 Al/*d6r*) but varying 6-MR Al arrangement, where "ipr" indicates that the sample was synthesized with Al-isopropoxide as the Al source. Conditions: 473 K, 1-60 kPa O_2, 0.03 kPa NO, 0.03 kPa NH_3, 7 kPa CO_2, 1 kPa H_2O, balance N_2. Trend lines for represent best-fits to Eqn. 2. The legend in panel a applies to panels a, b, and c.

Mechanistic interpretations of steady-state SCR kinetic data were corroborated by *operando* XAS measurements of Cu^{I} fractions on Cu-CHA zeolites of varying composition at 1, 10, and 60 kPa O_2 (Figure 2). *Operando* XAS data on samples of varying Cu density (at 0.6 Al/*d6r*) in our prior work[53] showed that SCR rates become increasingly limited by Cu^{II} reduction with increasing Cu density or O_2 pressure. New *operando* XAS data collected in this study on samples of varying Al density reveal important new insights. First, steady-state Cu^{I} fractions on low-Al density samples (0.2–0.8 Al/*d6r*) are comparable to those on samples studied previously (0.6 Al/*d6r*), when compared at similar Cu densities and O_2 pressures. Steady-state Cu^{I} fractions systematically decrease with increasing Al density (1.3–1.7 Al/*d6r*) beyond a threshold of >1 Al/*d6r* (as shown by data on samples at a fixed ~0.13 Cu/*d6r*), indicating that SCR rates are more Cu^{II} reduction-limited at the same reaction conditions. Given that the distribution of Cu oxidation states measured *in operando* reflect the balance between Cu^{I} oxidation and Cu^{II} reduction half-cycle rates during steady-state turnover,[5,53] these XAS data provide direct evidence of faster rates of Cu^{I} oxidation relative to Cu^{II} reduction at higher framework Al densities (>1 Al/*d6r*).

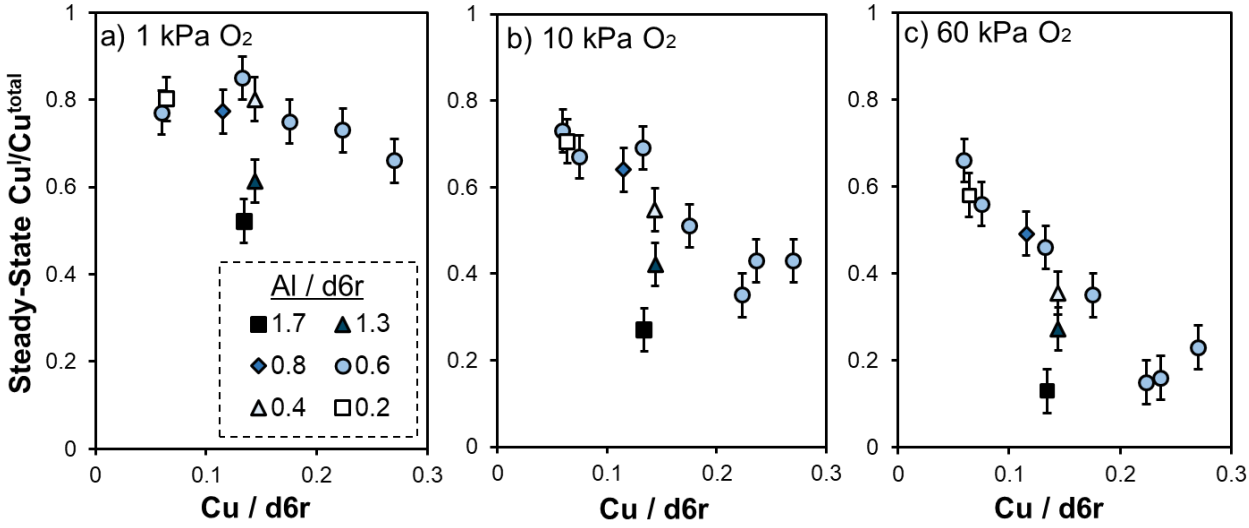

Figure 2. Steady-state Cu^{I} fractions measured by *operando* XAS on Cu-CHA samples of varying Cu and Al density at (a) 1, (b) 10, and (c) 60 kPa O_2 (0.03 kPa NO, 0.03 kPa NH_3, 7 kPa CO_2, 2.5 kPa H_2O, balance N_2). Associated XANES spectra are displayed in Figure S14, SI. Data from 0.6 Al/*d6r* series reproduced with permission from Jones et al.[53] The legend in panel a applies to the entire figure.

2.2. Effects of Framework Al Density on Cu^{I} Oxidation Kinetics

The interdependence of SCR rates on material composition and redox environment motivates isolation of the kinetic behavior associated with Cu^{I} oxidation and Cu^{II} reduction processes. SCR rates (Figure 1) were regressed to an empirical Langmuirian model (Eqn. 2) to extract apparent rate constants associated with kinetic regimes limited by Cu^{I} oxidation (k_{first}) and Cu^{II} reduction (k_{zero}), corresponding to the limits of low and high O_2 pressure, respectively; best fits are shown for each dataset in Figure 3.

$$\frac{-\mathrm{r_{NO}}}{[\mathrm{Cu}_{tot}]} = \frac{k_{first}\mathrm{k}_{zero}P_{O_2}}{k_{zero}+\mathrm{k}_{first}P_{O_2}} \qquad (Eqn.\ 2)$$

In this study, we use this mean-field equation (Eqn. 2) that normalizes SCR rates per total Cu sites in order to analyze the dependences of oxidation- and reduction-limited rate constants on Cu and Al density, which allows identifying when non-mean-field kinetic behavior is displayed.[4]

Values of k_{first} are shown in Figure 3a for Cu-CHA samples of varying Cu and Al density, and in Figure 3b as a function of Al density for samples of fixed Cu density of ~0.13 Cu/*d6r* (data at ~0.06 or ~0.23 Cu/*d6r* are displayed in Figure S11, SI and show similar trends). At fixed Al density, increasing the Cu density causes k_{first} values (per Cu) to increase systematically (Figure 3a), consistent with the dual-site requirement of Cu ion pairing during Cu^{I} oxidation.[5,53] At fixed Cu density, increasing the Al density (Figures 3b and S11, SI) leads to similar k_{first} values in the limit of dilute Al density (0.2–0.8 Al/*d6r*), but to significantly higher k_{first} values (5× higher for 1.7 than 0.4 Al/*d6r*, Figure 3b) at higher framework Al densities (>1 Al/*d6r*). The

higher Cu^{I} oxidation rate constants on such materials, in turn, lead to lower Cu^{I} fractions measured *in operando* at a given set of reaction conditions (Figure 2) as SCR rates become more limited by Cu^{II} reduction.

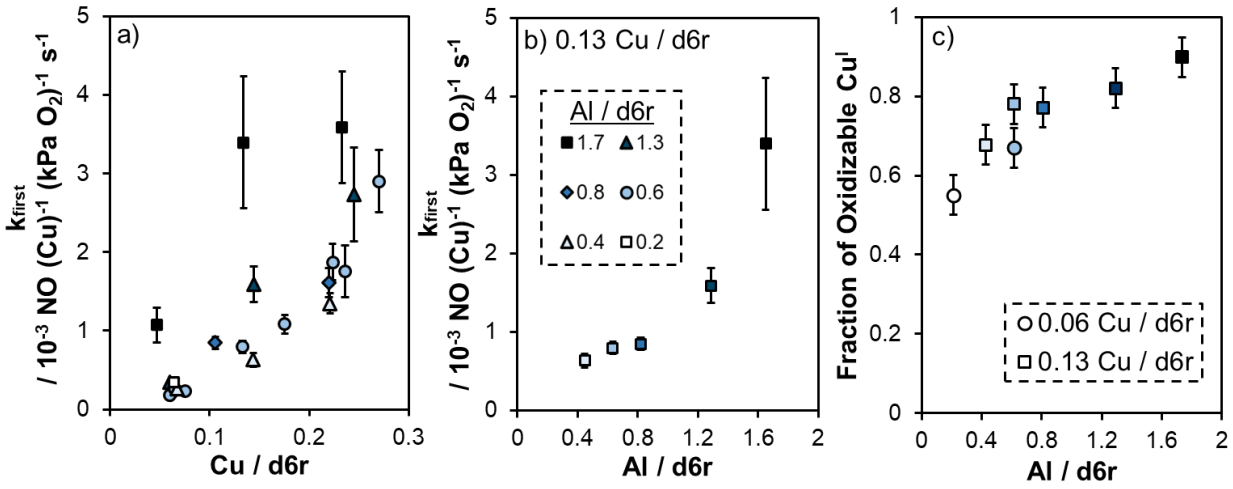

Figure 3. Cu^{I} oxidation kinetics and transient XAS (473 K) on Cu-CHA materials of varying composition. Dependence of k_{first} values on (a) Cu density for samples of varying Al density, and on (b) Al density for samples of fixed Cu density (0.13 Cu/*d6r*); legend for both panels shown in (b). (c) Fraction of Cu^{I} sites that oxidize in O_2 (10 kPa) measured by transient XAS, plotted alongside data from 0.6 Al/*d6r* series reproduced with permission from Jones et al.[53] Associated XANES spectra and spectro-kinetic traces shown in Figures S14 and S15 (SI, Section S4.3). The legend in panel b applies to panels a and b.

Figure 3c displays transient XAS data quantifying the fraction of $Cu^{I}(NH_3)_2$ complexes that are oxidized in O_2 (10 kPa, 473 K) at long times (full kinetic profiles provided in Figure S16, SI Section S4.3) and provides two important insights. First, at a fixed Cu density (0.06 Cu/*d6r*), decreasing the Al density from 0.6 to 0.2 Al/*d6r* results in a lower fraction of oxidizable Cu^{I} (0.67 to 0.55, respectively). Second, at a fixed Cu density (0.13 Cu/*d6r*), the fraction of oxidizable Cu^{I} increases systematically with Al density between 0.4–1.7 Al/*d6r*, approaching unity at the highest Al densities studied (0.90 for 1.7 Al/*d6r*, Figure 3c). Consistent with these findings, Borfecchia and co-workers recently reported that the fraction of oxidizable $Cu^{I}(NH_3)_2$

(473 K, 10 kPa O_2) in Cu-CHA (1.5–2.6 wt% Cu) increases with Al density among three samples in the composition range of Si/Al = 5–29 (Al/*d6r* = 0.4-2.0).[59]

We first discuss the weak dependence of k_{first} values (Figure 3a-b) and the fraction of oxidizable Cu^I (Figure 3c) on Al density in the dilute Al limit (0.2–0.8 Al/*d6r*). The SCR oxidation half-cycle involves pairing of two NH_3-solvated Cu^I ions and reaction with O_2 to form binuclear O_2-bridged Cu^I intermediates. If Cu^I ions were randomly distributed throughout the CHA framework for the samples studied here (<0.3 Cu/*d6r*), the experimentally observed fractions of O_2-oxidizable Cu (>0.5) would require intercage Cu migration during steady-state catalytic turnover.[5] Alternatively, Cu ions may initially undergo intercage migration to form Cu ion pairs that reside within a given cage at steady-state, thereby catalyzing SCR redox cycles without requiring intercage Cu migration; yet, this hypothesis is inconsistent with the significantly lower fraction of zeolite unit cells that contain multiple Al centers in the composition range studied (e.g., 0.15 for 0.2 Al/*d6r*; additional discussion in Section S5.2, SI) compared to the fractions of O_2-oxidizable Cu (>0.5) measured by XAS. The weak dependence of both k_{first} values (Figure 3a-b) and the fraction of O_2-oxidizable Cu (Figure 3c) on Al density in the dilute limit corroborates the hypothesis that Cu^I oxidation half-cycles involve intercage Cu ion migration during steady-state SCR turnover, and further implies that the rate of Cu^I ion migration is similar in the dilute framework Al limit.

Next, we interpret the increase in k_{first} values (Figure 3a-b) and fraction of oxidizable Cu^I (Figure 3c) with Al density for zeolite compositions that are more Al-dense (>1 Al/d6r). Given that Cu^I oxidation involves pairing of ionically-tethered Cu via intercage migration,[5] sufficiently high densities of anionic Al charges in the framework cause nearly all $Cu^I(NH_3)_2$ complexes to become catalytically active, thus increasing both steady-state Cu^I oxidation rates and the fraction

of O_2-oxidizable Cu^I. The observed 5× increase in k_{first} values with Al density between 0.4–1.7 Al/*d6r* (0.13 $Cu/_{d6r}$) greatly exceeds the increase in the fraction of oxidizable Cu sites (1.3×), implying that the rate of Cu^I oxidation per oxidizable Cu site increases significantly across this composition range.

Statistical simulations of proximity-dependent Cu pairing are shown in Figure 4 (details in Section 4.4 and SI, Section S2.3), with comparisons to experimentally quantified fractions of O_2-oxidizable Cu^I. Figure 4a reports the fractions of Cu ion pairs of minimum separation (Scheme 1) as a function of Cu density, at a fixed Al density of 0.6 Al/*d6r*. Even at the most dilute Cu densities studied here, a significant fraction of Cu ions share a common cage (Scheme 1a) and are accessible to each other via migration through local 8-MRs; this fraction grows rapidly with Cu density. The next largest fraction is Cu ion pairs separated by one cage (Scheme 1b), such that one Cu ion must migrate remotely from its anchoring Al to co-cage with another Cu ion. Figure 4a indicates consistency between simulation and experiment for the case where Cu sites are pairable if separated by up to one remote *cha* cage (Scheme 1b).[53] This interpretation is consistent with AIMD simulations indicating that Cu ions can migrate one *cha* cage away from the charge-balancing framework Al center with a free energy barrier of <60 kJ mol^{-1} when the destination cage does not contain Al,[5,42] an accessible barrier considering measured apparent activation barriers for low-temperature SCR are 40-80 kJ mol^{-1}.[40,60]

Figure 4b displays data for Cu-CHA materials of fixed Cu density (0.13 Cu/*d6r*) but varying Al density. At the highest Al density (1.7 Al/*d6r*), Figure 4b instead indicates consistency between simulation and experiment if Cu sites were pairable within two remote *cha* cages (Scheme 1c). Thus, we conclude that higher densities of anionic framework Al charges facilitate Cu^I ion migration over longer distances. Although Al density might indirectly influence

the kinetics or thermodynamics of O_2 adsorption at Cu^I sites, Cu^I ion pairing is proposed to be the dominant kinetically relevant step during the Cu^I oxidation half-cycle[5,43,44] and should be more affected by the electrostatic properties of the zeolite framework. We also considered and discarded the possibility that sufficiently high Al densities enable longer-range migration of NH_3-solvated Cu ions via solid-state ion exchange mechanisms[59,61,62] to form Cu pairs that permanently reside within a given *cha* cage (additional discussion in SI, Section S5.2).

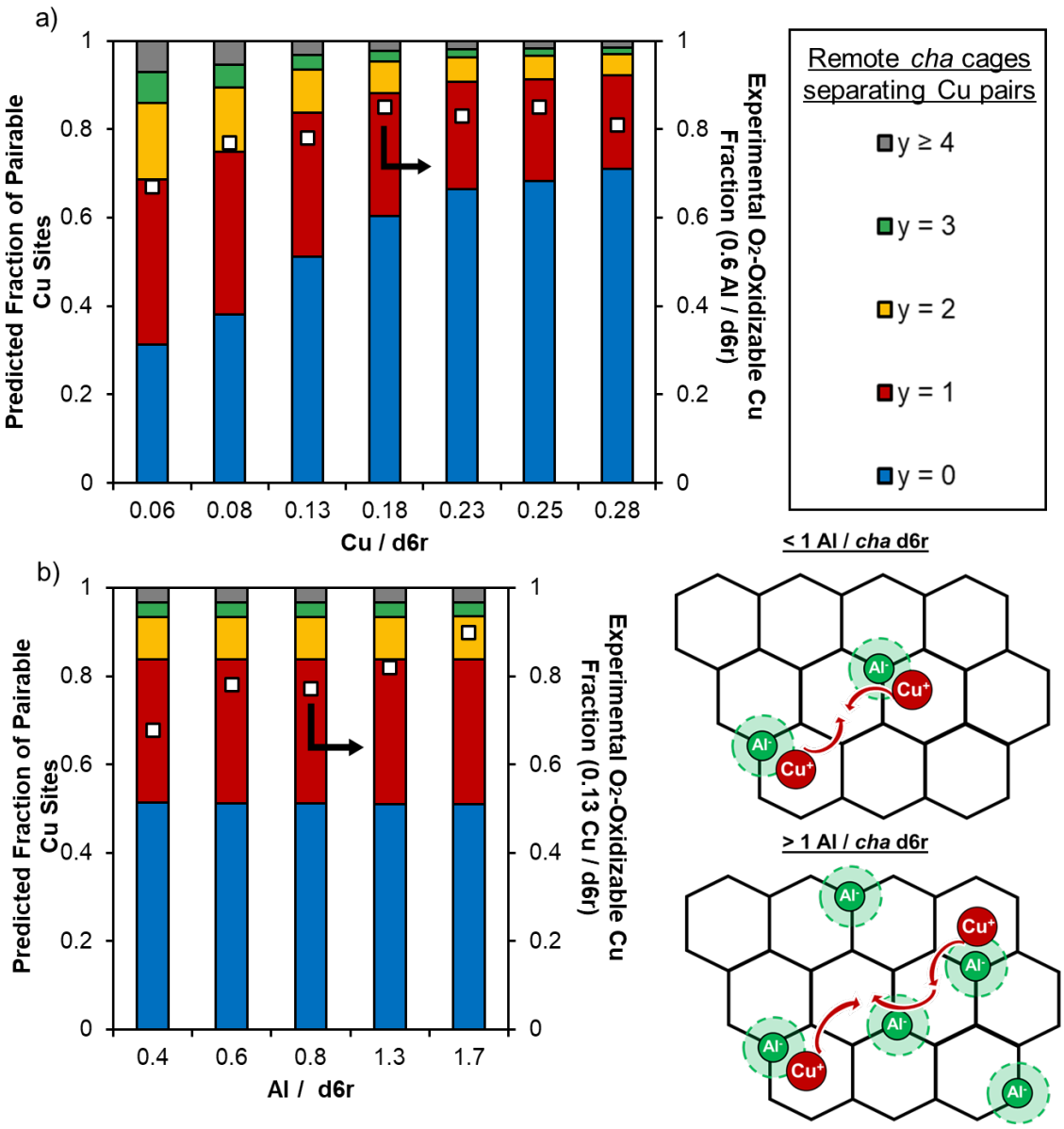

Figure 4. Statistically predicted fraction of pairable Cu sites versus (a) Cu and (b) Al density, as a function of the number of remote *cha* cages separating Cu site pairs. Right y-axis shows experimentally measured fraction of pairable $Cu^{I}(NH_3)_2$ sites in transient oxidation experiments (473 K, 10 kPa O_2): (a) at varying Cu density and a fixed Al density of 0.6 Al/*d6r*, reproduced from our previous work[53] ; (b) at varying Al density and a fixed Cu density of 0.13 Cu/*d6r*, with schematic representation of increased Cu ion mobility at higher framework Al densities.

2.3. Effects of Framework Al Density on Cu^{II} Reduction Kinetics

Values of k_{zero} are shown in Figure 5a for Cu-CHA samples of varying Cu and Al density, and in Figure 5b as a function of Al density for samples of fixed Cu density of ~0.13

Cu/*d6r* (data at ~0.06 and ~0.23 Cu/*d6r* are displayed in Figure S11, SI and show similar trends). For samples of fixed Al density, values of k_{zero} (per Cu) increase with a weakly positive dependence on Cu density (Figure 5a), consistent with prior reports of a single-site Cu^{II} reduction process[28] wherein the fraction of Cu sites that are SCR-active (i.e., O_2-oxidizable) increases with Cu density (additional discussion in SI, Section S5.3). While k_{zero} values are weakly dependent on Cu density (at fixed Al density), they display a maximum with respect to Al density (at fixed Cu density), a trend that is observed at sample compositions of both 0.13 and 0.22 Cu/*d6r* (Figure 5a). Maximal k_{zero} values are measured at 0.8 Al/*d6r*, while k_{zero} values are systematically lower (by 1.5–2×) at either higher or lower Al densities (Figure 5b), in sharp contrast to steady-state Cu^{I} oxidation kinetic data, for which k_{first} values increase monotonically with Al density (Figure 3b).

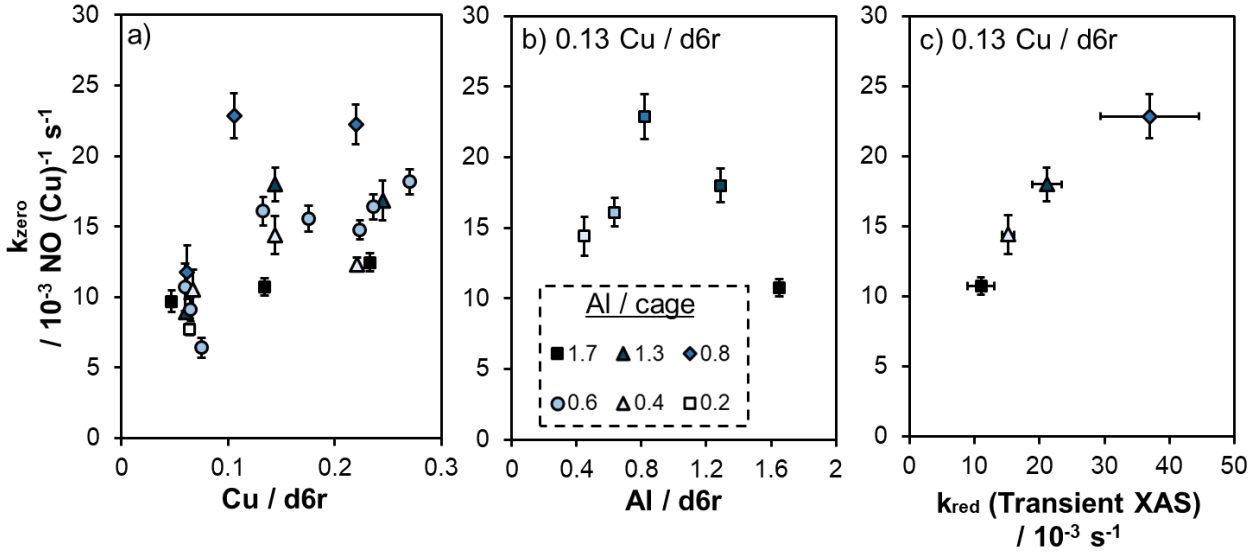

Figure 5. Cu^{II} reduction kinetics and transient XAS (473 K) on Cu-CHA materials of varying composition. Dependence of k_{zero} values on (a) Cu density for samples of varying Al density, and on (b) Al density for samples of fixed Cu density (0.13 Cu/*d6r*). (c) Steady-state reduction rate constant (k_{zero}, 473 K) plotted against the rate constant from transient XAS (k_{red}, 473 K) for the reduction of Cu^{II} intermediates by NO + NH_3 (0.03 kPa NO, 0.03 kPa NH_3, balance N_2), on samples of varying Al density but fixed Cu density (0.13 Cu/*d6r*). Associated experimental spectro-kinetic data and model fits provided in the SI, Section S4.4. The legend in panel b applies to the entire figure.

To determine whether such changes to apparent Cu^{II} reduction rate constants (k_{zero}; per total Cu) reflect changes to the intrinsic rate of Cu^{II} reduction or to the fraction of oxidizable Cu^{I} sites, we performed transient XAS measurements during reduction of binuclear NH_3-solvated Cu^{II} complexes by NO and NH_3. As shown in Figure S18 (SI, Section S4.4), transient reduction rates display first-order kinetics in Cu density (additional discussion in Section S5.3, SI). Data on samples with fixed Cu density show that intrinsic Cu^{II} reduction rate constants (k_{red}, per Cu) correlate positively with k_{zero} values measured from steady-state kinetics (Figure 5c), indicating that Al density subtly and non-monotonically influences the intrinsic rate of Cu^{II} reduction.

The maximal k_{zero} values at intermediate Al densities (Figure 5b) likely reflect a compensation between at least two effects. The increase in k_{zero} with increasing Al density in the dilute limit (<1 Al/*d6r*) likely reflects more facile Cu pairing over longer distances, as evidenced by the increasing fraction of pairable Cu^{I} measured in transient XAS oxidation experiments (Figure 3c); alternate less-likely hypotheses are discussed in the SI, Section S5.4. At higher Al densities (>1 Al/*d6r*), steady-state and transient kinetic data indicate that the Cu^{II} reduction rates become inhibited with increasing Al density (Figure 5). We simulated the number of NH_4^+ expected to share a given *cha* cage with Cu ions as a function of framework Al density (details provided in the SI, Section S2.2). While the majority of Cu are not co-caged with NH_4^+ at lower Al densities (e.g., 0.4 Al/*d6r*), the fraction of Cu with one co-caged NH_4^+ passes through a maximum near ~1 Al/*d6r*, beyond which the fraction of Cu with multiple NH_4^+ increases monotonically with Al density (Figure S8, SI). Thus, we hypothesize that the presence of more than one co-caged NH_4^+ inhibits Cu^{II} reduction rates. While the precise mechanistic origins of

such NH_4^+ inhibition effects remain unclear, we surmise they result from differences in Cu^{II} reduction pathways or energetics as a function of NH_4^+ density, or changing distributions of binuclear and mononuclear Cu^{II} species each with different barriers for subsequent reduction to $Cu^{I}(NH_3)_2$ (additional discussion in Section S5.5, SI). This proposal would be consistent with EXAFS data from Borfecchia et al. that Al density affects the structure of binuclear Cu^{II} complexes that form; lower Al densities (Si/Al = 29) favored bent binuclear complexes, while higher Al densities (Si/Al = 5) favored planar complexes with longer Cu-Cu distances.[59] These observations of Al density effects on Cu^{II} reduction kinetics motivate future work to identify the structures and energetics associated with various Cu^{II} species present during steady-state SCR conditions as a function of Cu-CHA composition.

3. Conclusions

Integration of experimental kinetics and *operando* spectroscopy with statistical simulations approach shows that anionic Al centers in zeolites regulate the mobility and reactivity of NH_3-solvated Cu ion sites that dynamically interact during NOx-SCR turnover. Cu ions within Cu-CHA samples of dilute framework Al density (<1 Al/*d6r*) display similar kinetic behavior and fractions of O_2-oxidizable Cu^{I} sites. In contrast, increasing the Al density (>1 Al/*d6r*) significantly increases the Cu^{I} oxidation rate and the fraction of O_2-oxidizable Cu^{I} sites, such that nearly all Cu ions are catalytically active at high Al densities (1.7 Al/*d6r*). Together with insights from statistical simulations that quantitatively predict the consequences of more facile Cu ion mobility on the fraction of pairable Cu sites, experimental kinetics and *operando* XAS data collected over CHA samples with widely varying Cu and Al compositions indicate Cu pairing occurs within one remote *cha* cage migration for samples of dilute Al content (<1

Al/d6r), but occurs within up to two remote *cha* cage migrations for samples of higher Al content (>1 Al/d6r). As a result, increasing the density of anionic charges localized at Al centers in zeolite lattices, which serve to ionically tether NH_3-solvated Cu ions, promotes their mobility and in turn increases rates of Cu ion migration and rate constants for reactions with dual-site requirements.

These findings have practical and mechanistic implications for NO_x-SCR. The redox environment in diesel NO_x-SCR aftertreatment systems changes with time and spatial position in catalyst monoliths during operation.[63–65] Our findings indicate that Cu-CHA zeolites with higher framework Al densities should be more resilient in maintaining higher NO_x conversion during transient excursions to low O_2 pressure, due to their higher Cu^I oxidation rate constants. In contrast, maintaining higher SCR rates under Cu^{II} reduction-limited conditions appear optimized at intermediate Al densities within the range of Cu densities studied here. More broadly, this work reveals new design principles within the emerging field of heterogeneous catalysis by mobilized metal ionic active sites, where both active site proximity (influenced by Cu density) and mobility (influenced by Al density) impact reactivity, and differently so for reactions with different site density requirements. While prior studies have investigated the non-mean-field kinetic behavior in NO_x-SCR by varying the spatial density of Cu sites on CHA zeolites of fixed Al density,[4,5,40,42,66] the comprehensive, composition-dependent kinetic and spectroscopic data presented here reveals that zeolitic framework Al anions are not simply a host for Cu cationic active sites; rather, the density of anionic Al centers significantly influences the kinetics of Cu^I oxidation and Cu^{II} reduction by regulating the mobility and reactivity of NH_3-solvated Cu ions during catalysis. Therefore, engineering bulk- and atomic-scale properties of zeolites can influence the mobility of Cu ions during NO_x-SCR; such parameters include the void

environment (i.e., framework topology)[67] and the spatial distribution of Cu cations, Al anions, and NH_4^+ or other co-cations present during catalysis.[68,69] This work also motivates further development of non-mean-field kinetic modeling[70] approaches to capture distance-dependent interactions between Cu sites. The conceptual framework and quantitative descriptions of framework Al density effects on Cu ion mobility for NO_X-SCR on Cu-zeolites are expected to be generalizable for catalyst systems operating by mechanisms of dynamic behavior of solvated metal cations ionically tethered to heterogeneous supports.

4. Methods

4.1. Zeolite synthesis and characterization

Parent CHA zeolites were synthesized by adapting previously reported procedures (details in Section S2.1, SI).[15,49–52] Cu-form zeolites were prepared via aqueous-phase Cu ion exchange of H-form zeolites using a $Cu^{II}(NO_3)_2$ solution, according to previously reported procedures (details in Section S2.2, SI).[5,15] The number of Al present in paired configurations within 6-MR of CHA (Al-O-Si-O-Al; Al-O-Si-O-Si-O-Al) was determined by Co^{2+} titration, according to previously reported methods (details in Section S2.2, SI).[51,52] All zeolites were characterized (Section S2.3) by X-ray diffraction (Figure S1, SI), Ar adsorption isotherms (Figure S2, Table S2, SI), elemental analysis by ICP-OES, ^{27}Al magic angle spinning nuclear magnetic resonance spectroscopy (Figure S3, Table S2, SI) and NH_3 temperature programmed desorption (Table S1, Table S3, SI).

4.2. Measurement of standard SCR kinetics under differential conditions

NO_x selective catalytic reduction (SCR) kinetic data were measured using a tubular quartz reactor system described previously[29], and using experimental methods described previously; additional details are provided in Section S3, SI.[53,60] The total gas flow rate was 16.7–41.7 $cm^3\ s^{-1}$ (at ambient temperature and pressure) and the mass of CHA solids was 0.0109–0.0605 g, chosen to maintain differential NO conversion (<20%). Outlet NO, NO_2, NH_3, CO_2, and H_2O concentrations were measured every 0.95 s using on-board gas calibrations on a gas-phase Fourier Transform Infrared (FTIR) spectrometer (MKS Multigas™ 2030). The rate of "standard" SCR (involving O_2 as the oxidant) was determined by correcting the overall rate of NO consumption measured in each experiment for contributions to NO consumption resulting from "fast" SCR reactions with NO_2, present both as an impurity in NO gas cylinders and formed via gas-phase NO oxidation reactions within the reactor unit.[53] SCR rates are independent of external and intracrystalline transport artifacts, as shown in our previous work.[53] SCR rates were shown to be independent of H_2O (0.2–4 kPa)[5,71] and CO_2 (0–16 kPa) [29,71] pressures in our previous work.

4.3. Operando and transient X-ray absorption spectroscopic characterization of Cu-CHA

X-ray absorption spectroscopy (XAS) experiments were carried out at the Advanced Photon Source (APS) at Argonne National Laboratory on the insertion device (ID) beam line of the Materials Research Collaborative Access Team (MRCAT, Sector 10), [72] and XAS data were processed in ATHENA.[73] Experimental details are provided in the SI, Section S4.1. Linear combination fitting (LCF) of the XANES spectra (473 K) was performed using standards for Cu^{I} (Cu-CHA zeolite reduced in NO and NH_3 at 473 K) and Cu^{II} (Cu-CHA zeolite oxidized in 20

kPa O_2 at 673 K)[74] to determine the fractions of Cu^I and Cu^{II} species present (reference XAS spectra are shown in Figure S13, SI). LCF used the energy range (-20) to (+30) eV (E_0 = 8982.0 eV), and fits were constrained such that the fractions of each species sum to unity. Experimental error for measurements of Cu^I and Cu^{II} fractions was taken as ± 0.05 based on confidence intervals provided in LCF fits, and verified through triplicate spectra for steady-state measurements.[53]

Operando XAS experiments were performed in a glassy carbon tube reactor described previously,[75] in which steady-state SCR rate measurements were collected simultaneously with XAS spectra to verify that rates were similar to those measured in separate, differential laboratory reactor experiments. Multiple spectra were taken to confirm the absence of beam damage to the sample or any other time-dependent changes. Transient O_2 oxidation experiments were carried out following complete reduction of Cu-CHA samples to the $Cu^I(NH_3)_2$ state (0.03 kPa NO, 0.03 kPa NH3, balance N_2, 473 K, 13.3 $cm^3\ s^{-1}$). After purging in flowing N_2 (13.3 $cm^3\ s^{-1}$) for 0.08 hr, flowing O_2 (10 kPa in N_2, 13.3 $cm^3\ s^{-1}$) was introduced concurrently with the start of collecting XAS spectra. Following the O_2 oxidation transients which form binuclear Cu^{II} intermediates (while spatially isolated Cu^I sites remain un-oxidized), transient NO and NH_3 reduction experiments were carried out at 473 K. After purging for 0.08 h in flowing N_2 (13.3 $cm^3\ s^{-1}$), flowing NH_3 (0.03 kPa in balance N_2, 13.3 $cm^3\ s^{-1}$) was introduced to the sample. Shortly thereafter (approximately 0.01-0.08 h), flowing NO was added to the gas stream (0.03 kPa NO, 0.03 kPa NH_3, balance N_2, 13.3 $cm^3\ s^{-1}$) concurrently with the start of collecting XAS spectra. For both reduction and oxidation transient experiments, spectra were collected until changes were no longer detectable as a function of time.

4.4. Statistical simulations of Cu-Cu proximity

The fraction of Cu ions that can pair via migrations through different numbers of remote *cha* cages were assessed as a function of bulk Cu and Al densities, to compare to the experimentally measured fraction of oxidizable Cu^{I} (Figure 4; additional details provided in SI, Section S2.3). Cu ions are assumed to be randomly distributed at framework Al, and "local" migration into adjacent *cha* cages via 8-MR windows containing the charge-balancing Al center is assumed to be facile.[5,42,76] In the first iteration, Cu site pairs with charge-balancing Al belonging to the same 36-T-site unit cell are quantified, which corresponds to local Cu ion migration. Subsequent iterations (2-4) quantify Cu pairs separated by one, two, or three remote *cha* cages. Following the fourth iteration, all remaining unpaired Cu sites are separated by four or more remote *cha* cages.

5. Acknowledgments

We acknowledge financial support provided by the National Science Foundation DMREF program under award number 1922173-CBET. Use of the Advanced Photon Source is supported by the U.S. Department of Energy, Office of Science, and Office of Basic Energy Sciences, under contract no. DE-AC02-06CH11357. MRCAT operations and beamline 10-ID are supported by the Department of Energy and the MRCAT member institutions. We thank Prof. Christopher Paolucci (Virginia) for helpful technical discussions. We thank Sachem, Inc. for providing the organic structure-directing agent used to synthesize SSZ-13. We thank Dr. John Harwood (Purdue Interdepartmental NMR Facility) for assistance collecting NMR spectra.

6. References

(1) Hinshelwood, C. N. *The Kinetics of Chemical Change,*; The Clarendon Press: Oxford, 1940.

(2) Langmuir, I. Part II.—"Heterogeneous Reactions". Chemical Reactions on Surfaces. *Trans. Faraday Soc.* **1922**, *17* (0), 607–620. https://doi.org/10.1039/TF9221700607.

(3) Hougen, O. A.; Watson, K. M. Solid Catalysts and Reaction Rates - General Principles. *Ind. Eng. Chem.* **1943**, *35* (5), 529–541. https://doi.org/10.1021/ie50401a005.

(4) Krishna, S. H.; Jones, C. B.; Gounder, R. Dynamic Interconversion of Metal Active Site Ensembles in Zeolite Catalysis. *Annu. Rev. Chem. Biomol. Eng.* **2021**, *12* (1), 115–136. https://doi.org/10.1146/annurev-chembioeng-092120-010920.

(5) Paolucci, C.; Khurana, I.; Parekh, A. A.; Li, S.; Shih, A. J.; Li, H.; Di Iorio, J. R.; Albarracin-Caballero, J. D.; Yezerets, A.; Miller, J. T.; Delgass, W. N.; Ribeiro, F. H.; Schneider, W. F.; Gounder, R. Dynamic Multinuclear Sites Formed by Mobilized Copper Ions in NO$_x$</Em> Selective Catalytic Reduction. *Science* **2017**, *357* (6354), 898–903. https://doi.org/10.1126/science.aan5630.

(6) Dinh, K. T.; Sullivan, M. M.; Narsimhan, K.; Serna, P.; Meyer, R. J.; Dincă, M.; Román-Leshkov, Y. Continuous Partial Oxidation of Methane to Methanol Catalyzed by Diffusion-Paired Copper Dimers in Copper-Exchanged Zeolites. *J. Am. Chem. Soc.* **2019**, *141* (29), 11641–11650. https://doi.org/10.1021/jacs.9b04906.

(7) Zhang, Z.; Zandkarimi, B.; Alexandrova, A. N. Ensembles of Metastable States Govern Heterogeneous Catalysis on Dynamic Interfaces. *Acc. Chem. Res.* **2020**, *53* (2), 447–458. https://doi.org/10.1021/acs.accounts.9b00531.

(8) Zugic, B.; Wang, L.; Heine, C.; Zakharov, D. N.; Lechner, B. A. J.; Stach, E. A.; Biener, J.; Salmeron, M.; Madix, R. J.; Friend, C. M. Dynamic Restructuring Drives Catalytic Activity on Nanoporous Gold–Silver Alloy Catalysts. *Nat. Mater.* **2017**, *16* (5), 558–564. https://doi.org/10.1038/nmat4824.

(9) Wang, Y.-G.; Mei, D.; Glezakou, V.-A.; Li, J.; Rousseau, R. Dynamic Formation of Single-Atom Catalytic Active Sites on Ceria-Supported Gold Nanoparticles. *Nat. Commun.* **2015**, *6* (1), 6511. https://doi.org/10.1038/ncomms7511.

(10) Tang, Y.; Asokan, C.; Xu, M.; Graham, G. W.; Pan, X.; Christopher, P.; Li, J.; Sautet, P. Rh Single Atoms on TiO2 Dynamically Respond to Reaction Conditions by Adapting Their Site. *Nat. Commun.* **2019**, *10* (1), 4488. https://doi.org/10.1038/s41467-019-12461-6.

(11) Resasco, J.; Dai, S.; Graham, G.; Pan, X.; Christopher, P. Combining In-Situ Transmission Electron Microscopy and Infrared Spectroscopy for Understanding Dynamic and Atomic-Scale Features of Supported Metal Catalysts. *J. Phys. Chem. C* **2018**, *122* (44), 25143–25157. https://doi.org/10.1021/acs.jpcc.8b03959.

(12) Liu, L.; Corma, A. Confining Isolated Atoms and Clusters in Crystalline Porous Materials for Catalysis. *Nat. Rev. Mater.* **2020**. https://doi.org/10.1038/s41578-020-00250-3.

(13) Paolucci, C.; Di Iorio, J. R.; Schneider, W. F.; Gounder, R. Solvation and Mobilization of Copper Active Sites in Zeolites by Ammonia: Consequences for the Catalytic Reduction of Nitrogen Oxides. *Acc. Chem. Res.* **2020**, *53* (9), 1881–1892. https://doi.org/10.1021/acs.accounts.0c00328.

(14) Mandal, K.; Gu, Y.; Westendorff, K. S.; Li, S.; Pihl, J. A.; Grabow, L. C.; Epling, W. S.; Paolucci, C. Condition-Dependent Pd Speciation and NO Adsorption in Pd/Zeolites. *ACS Catal.* **2020**, *10* (21), 12801–12818. https://doi.org/10.1021/acscatal.0c03585.

(15) Paolucci, C.; Parekh, A. A.; Khurana, I.; Di Iorio, J. R.; Li, H.; Albarracin Caballero, J. D.; Shih, A. J.; Anggara, T.; Delgass, W. N.; Miller, J. T.; Ribeiro, F. H.; Gounder, R.; Schneider, W. F. Catalysis in a Cage: Condition-Dependent Speciation and Dynamics of Exchanged Cu Cations in SSZ-13 Zeolites. *J. Am. Chem. Soc.* **2016**, *138* (18), 6028–6048. https://doi.org/10.1021/jacs.6b02651.
(16) Janssens, T. V. W.; Falsig, H.; Lundegaard, L. F.; Vennestrøm, P. N. R.; Rasmussen, S. B.; Moses, P. G.; Giordanino, F.; Borfecchia, E.; Lomachenko, K. A.; Lamberti, C.; Bordiga, S.; Godiksen, A.; Mossin, S.; Beato, P. A Consistent Reaction Scheme for the Selective Catalytic Reduction of Nitrogen Oxides with Ammonia. *ACS Catal.* **2015**, *5* (5), 2832–2845. https://doi.org/10.1021/cs501673g.
(17) Lomachenko, K. A.; Borfecchia, E.; Negri, C.; Berlier, G.; Lamberti, C.; Beato, P.; Falsig, H.; Bordiga, S. The Cu-CHA DeNOx Catalyst in Action: Temperature-Dependent NH3-Assisted Selective Catalytic Reduction Monitored by Operando XAS and XES. *J. Am. Chem. Soc.* **2016**, *138* (37), 12025–12028. https://doi.org/10.1021/jacs.6b06809.
(18) Brogaard, R. Y.; Kømurcu, M.; Dyballa, M. M.; Botan, A.; Van Speybroeck, V.; Olsbye, U.; De Wispelaere, K. Ethene Dimerization on Zeolite-Hosted Ni Ions: Reversible Mobilization of the Active Site. *ACS Catal.* **2019**, *9* (6), 5645–5650. https://doi.org/10.1021/acscatal.9b00721.
(19) Imbao, J.; van Bokhoven, J. A.; Clark, A.; Nachtegaal, M. Elucidating the Mechanism of Heterogeneous Wacker Oxidation over Pd-Cu/Zeolite Y by Transient XAS. *Nat. Commun.* **2020**, *11* (1), 1118. https://doi.org/10.1038/s41467-020-14982-x.
(20) Espeel, P. H.; De Peuter, G.; Tielen, M. C.; Jacobs, P. A. Mechanism of the Wacker Oxidation of Alkenes over Cu-Pd-Exchanged Y Zeolites. *J. Phys. Chem.* **1994**, *98* (44), 11588–11596. https://doi.org/10.1021/j100095a047.
(21) Signorile, M.; Borfecchia, E.; Bordiga, S.; Berlier, G. Influence of Ion Mobility on the Redox and Catalytic Properties of Cu Ions in Zeolites. *Chem. Sci.* **2022**. https://doi.org/10.1039/D2SC03565K.
(22) Gounder, R.; Moini, A. Automotive NOx Abatement Using Zeolite-Based Technologies. *React. Chem. Eng.* **2019**, *4* (6), 966–968. https://doi.org/10.1039/c9re90030f.
(23) Lambert, C. K. Perspective on SCR NOx Control for Diesel Vehicles. *React. Chem. Eng.* **2019**, *4* (6), 969–974. https://doi.org/10.1039/C8RE00284C.
(24) Peden, C. H. F. Cu/Chabazite Catalysts for 'Lean-Burn' Vehicle Emission Control. *J. Catal.* **2019**, *373*, 384–389. https://doi.org/10.1016/j.jcat.2019.04.046.
(25) Badshah, H.; Posada, F.; Muncrief, R. *Current State of NOx Emissions from In-Use Heavy-Duty Diesel Vehicles in the United States*; White Paper; International Council on Clean Transportation, 2019.
(26) Krishna, S. H.; Jones, C. B.; Miller, J. T.; Ribeiro, F. H.; Gounder, R. Combining Kinetics and Operando Spectroscopy to Interrogate the Mechanism and Active Site Requirements of NOx Selective Catalytic Reduction with NH3 on Cu-Zeolites. *J. Phys. Chem. Lett.* **2020**, *11* (13), 5029–5036. https://doi.org/10.1021/acs.jpclett.0c00903.
(27) Deka, U.; Juhin, A.; Eilertsen, E. A.; Emerich, H.; Green, M. A.; Korhonen, S. T.; Weckhuysen, B. M.; Beale, A. M. Confirmation of Isolated Cu2+ Ions in SSZ-13 Zeolite as Active Sites in NH3-Selective Catalytic Reduction. *J. Phys. Chem. C* **2012**, *116* (7), 4809–4818. https://doi.org/10.1021/jp212450d.
(28) Paolucci, C.; Verma, A. A.; Bates, S. A.; Kispersky, V. F.; Miller, J. T.; Gounder, R.; Delgass, W. N.; Ribeiro, F. H.; Schneider, W. F. Isolation of the Copper Redox Steps in the

Standard Selective Catalytic Reduction on Cu-SSZ-13. *Angew. Chem. Int. Ed.* **2014**, *53* (44), 11828–11833. https://doi.org/10.1002/anie.201407030.
(29) Bates, S. A.; Verma, A. A.; Paolucci, C.; Parekh, A. A.; Anggara, T.; Yezerets, A.; Schneider, W. F.; Miller, J. T.; Delgass, W. N.; Ribeiro, F. H. Identification of the Active Cu Site in Standard Selective Catalytic Reduction with Ammonia on Cu-SSZ-13. *J. Catal.* **2014**, *312*, 87–97.
(30) Kispersky, V. F.; Kropf, A. J.; Ribeiro, F. H.; Miller, J. T. Low Absorption Vitreous Carbon Reactors for OperandoXAS: A Case Study on Cu/Zeolites for Selective Catalytic Reduction of NOx by NH3. *Phys. Chem. Chem. Phys.* **2012**, *14* (7), 2229–2238. https://doi.org/10.1039/c1cp22992c.
(31) Wang, X.; Chen, L.; Vennestrøm, P. N. R.; Janssens, T. V. W.; Jansson, J.; Grönbeck, H.; Skoglundh, M. Direct Measurement of Enthalpy and Entropy Changes in NH3 Promoted O2 Activation over Cu-CHA at Low Temperature. *ChemCatChem* **2021**, *13*, 2577. https://doi.org/10.1002/cctc.202100253.
(32) Luo, J.; Gao, F.; Kamasamudram, K.; Currier, N.; Peden, C. H. F.; Yezerets, A. New Insights into Cu/SSZ-13 SCR Catalyst Acidity. Part I: Nature of Acidic Sites Probed by NH3 Titration. *J. Catal.* **2017**, *348*, 291–299. https://doi.org/10.1016/j.jcat.2017.02.025.
(33) Giordanino, F.; Borfecchia, E.; Lomachenko, K. A.; Lazzarini, A.; Agostini, G.; Gallo, E.; Soldatov, A. V.; Beato, P.; Bordiga, S.; Lamberti, C. Interaction of NH3 with Cu-SSZ-13 Catalyst: A Complementary FTIR, XANES, and XES Study. *J. Phys. Chem. Lett.* **2014**, *5* (9), 1552–1559. https://doi.org/10.1021/jz500241m.
(34) Negri, C.; Selleri, T.; Borfecchia, E.; Martini, A.; Lomachenko, K. A.; Janssens, T. V. W.; Cutini, M.; Bordiga, S.; Berlier, G. Structure and Reactivity of Oxygen-Bridged Diamino Dicopper(II) Complexes in Cu-Ion-Exchanged Chabazite Catalyst for NH3-Mediated Selective Catalytic Reduction. *J. Am. Chem. Soc.* **2020**, *142* (37), 15884–15896. https://doi.org/10.1021/jacs.0c06270.
(35) McCann, S. D.; Stahl, S. S. Copper-Catalyzed Aerobic Oxidations of Organic Molecules: Pathways for Two-Electron Oxidation with a Four-Electron Oxidant and a One-Electron Redox-Active Catalyst. *Acc. Chem. Res.* **2015**, *48* (6), 1756–1766. https://doi.org/10.1021/acs.accounts.5b00060.
(36) Hoover, J. M.; Ryland, B. L.; Stahl, S. S. Mechanism of Copper(I)/TEMPO-Catalyzed Aerobic Alcohol Oxidation. *J. Am. Chem. Soc.* **2013**, *135* (6), 2357–2367. https://doi.org/10.1021/ja3117203.
(37) Solomon, E. I.; Heppner, D. E.; Johnston, E. M.; Ginsbach, J. W.; Cirera, J.; Qayyum, M.; Kieber-Emmons, M. T.; Kjaergaard, C. H.; Hadt, R. G.; Tian, L. Copper Active Sites in Biology. *Chem. Rev.* **2014**, *114* (7), 3659–3853. https://doi.org/10.1021/cr400327t.
(38) Solomon, E. I.; Ginsbach, J. W.; Heppner, D. E.; Kieber-Emmons, M. T.; Kjaergaard, C. H.; Smeets, P. J.; Tian, L.; Woertink, J. S. Copper Dioxygen (Bio)Inorganic Chemistry. *Faraday Discuss.* **2011**, *148* (0), 11–39. https://doi.org/10.1039/C005500J.
(39) Gao, F.; Walter, E. D.; Kollar, M.; Wang, Y.; Szanyi, J.; Peden, C. H. F. Understanding Ammonia Selective Catalytic Reduction Kinetics over Cu/SSZ-13 from Motion of the Cu Ions. *J. Catal.* **2014**, *319*, 1–14. https://doi.org/10.1016/j.jcat.2014.08.010.
(40) Gao, F.; Mei, D.; Wang, Y.; Szanyi, J.; Peden, C. H. F. Selective Catalytic Reduction over Cu/SSZ-13: Linking Homo- and Heterogeneous Catalysis. *J. Am. Chem. Soc.* **2017**, *139* (13), 4935–4942. https://doi.org/10.1021/jacs.7b01128.

(41) Liu, C.; Kubota, H.; Amada, T.; Kon, K.; Toyao, T.; Maeno, Z.; Ueda, K.; Ohyama, J.; Satsuma, A.; Tanigawa, T.; Tsunoji, N.; Sano, T.; Shimizu, K. In Situ Spectroscopic Studies on the Redox Cycle of NH3–SCR over Cu-CHA Zeolites. *ChemCatChem* **2020**, *12* (11), 3050–3059. https://doi.org/10.1002/cctc.202000024.
(42) Millan, R.; Cnudde, P.; van Speybroeck, V.; Boronat, M. Mobility and Reactivity of Cu+ Species in Cu-CHA Catalysts under NH3-SCR-NOx Reaction Conditions: Insights from AIMD Simulations. *JACS Au* **2021**, *1* (10), 1778–1787. https://doi.org/10.1021/jacsau.1c00337.
(43) Chen, L.; Falsig, H.; Janssens, T. V. W.; Grönbeck, H. Activation of Oxygen on (NH3CuNH3)+ in NH3-SCR over Cu-CHA. *J. Catal.* **2018**, *358*, 179–186. https://doi.org/10.1016/j.jcat.2017.12.009.
(44) Liu, C.; Kubota, H.; Toyao, T.; Maeno, Z.; Shimizu, K. Mechanistic Insights into the Oxidation of Copper(I) Species during NH3–SCR over Cu-CHA Zeolites: A DFT Study. *Catal. Sci. Technol.* **2020**, *10*, 3586–3593. https://doi.org/10.1039/D0CY00379D.
(45) Gao, F.; Washton, N. M.; Wang, Y.; Kollár, M.; Szanyi, J.; Peden, C. H. F. Effects of Si/Al Ratio on Cu/SSZ-13 NH3-SCR Catalysts: Implications for the Active Cu Species and the Roles of Brønsted Acidity. *J. Catal.* **2015**, *331*, 25–38. https://doi.org/10.1016/j.jcat.2015.08.004.
(46) Godiksen, A.; Isaksen, O. L.; Rasmussen, S. B.; Vennestrøm, P. N. R.; Mossin, S. Site-Specific Reactivity of Copper Chabazite Zeolites with Nitric Oxide, Ammonia, and Oxygen. *ChemCatChem* **2018**, *10* (2), 366–370. https://doi.org/10.1002/cctc.201701357.
(47) Lee, H.; Song, I.; Jeon, S. W.; Kim, D. H. Mobility of Cu Ions in Cu-SSZ-13 Determines the Reactivity of Selective Catalytic Reduction of NOx with NH3. *J. Phys. Chem. Lett.* **2021**, 3210–3216. https://doi.org/10.1021/acs.jpclett.1c00181.
(48) Lee, H.; Song, I.; Jeon, S. W.; Kim, D. H. Control of the Cu Ion Species in Cu-SSZ-13 via the Introduction of Co2+ Co-Cations to Improve the NH3-SCR Activity. *Catal. Sci. Technol.* **2021**, *11*, 4838–4848. https://doi.org/10.1039/D1CY00623A.
(49) Fickel, D. W.; D'Addio, E.; Lauterbach, J. A.; Lobo, R. F. The Ammonia Selective Catalytic Reduction Activity of Copper-Exchanged Small-Pore Zeolites. *Appl. Catal. B Environ.* **2011**, *102* (3), 441–448. https://doi.org/10.1016/j.apcatb.2010.12.022.
(50) Zones, S. I. Zeolite SSZ-13 and Its Method of Preparation. US4544538A, 1985.
(51) Di Iorio, J. R.; Gounder, R. Controlling the Isolation and Pairing of Aluminum in Chabazite Zeolites Using Mixtures of Organic and Inorganic Structure-Directing Agents. *Chem. Mater.* **2016**, *28* (7), 2236–2247. https://doi.org/10.1021/acs.chemmater.6b00181.
(52) Di Iorio, J. R.; Nimlos, C. T.; Gounder, R. Introducing Catalytic Diversity into Single-Site Chabazite Zeolites of Fixed Composition via Synthetic Control of Active Site Proximity. *ACS Catal.* **2017**, *7* (10), 6663–6674. https://doi.org/10.1021/acscatal.7b01273.
(53) Jones, C. B.; Khurana, I.; Krishna, S. H.; Shih, A. J.; Delgass, W. N.; Miller, J. T.; Ribeiro, F. H.; Schneider, W. F.; Gounder, R. Effects of Dioxygen Pressure on Rates of NOx Selective Catalytic Reduction with NH3 on Cu-CHA Zeolites. *J. Catal.* **2020**, *389*, 140–149. https://doi.org/10.1016/j.jcat.2020.05.022.
(54) Oda, A.; Shionoya, H.; Hotta, Y.; Takewaki, T.; Sawabe, K.; Satsuma, A. Spectroscopic Evidence of Efficient Generation of Dicopper Intermediate in Selective Catalytic Reduction of NO over Cu-Ion-Exchanged Zeolites. *ACS Catal.* **2020**, 12333–12339. https://doi.org/10.1021/acscatal.0c03425.

(55) Greenaway, A. G.; Marberger, A.; Thetford, A.; Lezcano-González, I.; Agote-Arán, M.; Nachtegaal, M.; Ferri, D.; Kröcher, O.; Catlow, C. R. A.; Beale, A. M. Detection of Key Transient Cu Intermediates in SSZ-13 during NH3-SCR DeNOx by Modulation Excitation IR Spectroscopy. *Chem. Sci.* **2020**, *11* (2), 447–455. https://doi.org/10.1039/c9sc04905c.
(56) Fahami, A. R.; Günter, T.; Doronkin, D. E.; Casapu, M.; Zengel, D.; Vuong, T. H.; Simon, M.; Breher, F.; Kucherov, A. V.; Brückner, A.; Grunwaldt, J. D. The Dynamic Nature of Cu Sites in Cu-SSZ-13 and the Origin of the Seagull NOx Conversion Profile during NH3-SCR. *React. Chem. Eng.* **2019**, *4* (6), 1000–1018. https://doi.org/10.1039/c8re00290h.
(57) Feng, Y.; Wang, X.; Janssens, T. V. W.; Vennestrøm, P. N. R.; Jansson, J.; Skoglundh, M.; Grönbeck, H. First-Principles Microkinetic Model for Low-Temperature NH3-Assisted Selective Catalytic Reduction of NO over Cu-CHA. *ACS Catal.* **2021**, *11* (23), 14395–14407. https://doi.org/10.1021/acscatal.1c03973.
(58) Marberger, A.; Petrov, A. W.; Steiger, P.; Elsener, M.; Kröcher, O.; Nachtegaal, M.; Ferri, D. Time-Resolved Copper Speciation during Selective Catalytic Reduction of NO on Cu-SSZ-13. *Nat. Catal.* **2018**, *1* (3), 221–227. https://doi.org/10.1038/s41929-018-0032-6.
(59) Martini, A.; Negri, C.; Bugarin, L.; Deplano, G.; Abasabadi, R. K.; Lomachenko, K. A.; Janssens, T. V. W.; Bordiga, S.; Berlier, G.; Borfecchia, E. Assessing the Influence of Zeolite Composition on Oxygen-Bridged Diamino Dicopper(II) Complexes in Cu-CHA DeNOx Catalysts by Machine Learning-Assisted X-Ray Absorption Spectroscopy. *J. Phys. Chem. Lett.* **2022**, 6164–6170. https://doi.org/10.1021/acs.jpclett.2c01107.
(60) Krishna, S. H.; Jones, C. B.; Gounder, R. Temperature Dependence of Cu(I) Oxidation and Cu(II) Reduction Kinetics in the Selective Catalytic Reduction of NOx with NH3 on Cu-Chabazite Zeolites. *J. Catal.* **2021**, *404*, 873–882. https://doi.org/10.1016/j.jcat.2021.08.042.
(61) Shwan, S.; Skoglundh, M.; Lundegaard, L. F.; Tiruvalam, R. R.; Janssens, T. V. W.; Carlsson, A.; Vennestrøm, P. N. R. Solid-State Ion-Exchange of Copper into Zeolites Facilitated by Ammonia at Low Temperature. *ACS Catal.* **2015**, *5* (1), 16–19. https://doi.org/10.1021/cs5015139.
(62) Vennestrøm, P. N. R.; Lundegaard, L. F.; Tyrsted, C.; Bokarev, D. A.; Mytareva, A. I.; Baeva, G. N.; Stakheev, A. Y.; Janssens, T. V. W. The Role of Protons and Formation Cu(NH3)2+ During Ammonia-Assisted Solid-State Ion Exchange of Copper(I) Oxide into Zeolites. *Top. Catal.* **2019**, *62* (1), 100–107. https://doi.org/10.1007/s11244-018-1096-x.
(63) Cavataio, G.; Girard, J.; Patterson, J. E.; Montreuil, C.; Cheng, Y.; Lambert, C. K. Laboratory Testing of Urea-SCR Formulations to Meet Tier 2 Bin 5 Emissions. In *SAE World Congress & Exhibition*; SAE International, 2007. https://doi.org/10.4271/2007-01-1575.
(64) Doronkin, D. E.; Casapu, M.; Günter, T.; Müller, O.; Frahm, R.; Grunwaldt, J.-D. Operando Spatially- and Time-Resolved XAS Study on Zeolite Catalysts for Selective Catalytic Reduction of NOx by NH3. *J. Phys. Chem. C* **2014**, *118* (19), 10204–10212. https://doi.org/10.1021/jp5028433.
(65) Becher, J.; Sanchez, D. F.; Doronkin, D. E.; Zengel, D.; Meira, D. M.; Pascarelli, S.; Grunwaldt, J.-D.; Sheppard, T. L. Chemical Gradients in Automotive Cu-SSZ-13 Catalysts for NOx Removal Revealed by Operando X-Ray Spectrotomography. *Nat. Catal.* **2021**, *4*, 46–53. https://doi.org/10.1038/s41929-020-00552-3.

(66) Chen, L.; Janssens, T. V. W.; Vennestrøm, P. N. R.; Jansson, J.; Skoglundh, M.; Grönbeck, H. A Complete Multisite Reaction Mechanism for Low-Temperature NH3-SCR over Cu-CHA. *ACS Catal.* **2020**, *10* (10), 5646–5656. https://doi.org/10.1021/acscatal.0c00440.
(67) Tarach, K. A.; Jabłońska, M.; Pyra, K.; Liebau, M.; Reiprich, B.; Gläser, R.; Góra-Marek, K. Effect of Zeolite Topology on NH3-SCR Activity and Stability of Cu-Exchanged Zeolites. *Appl. Catal. B Environ.* **2021**, *284*, 119752. https://doi.org/10.1016/j.apcatb.2020.119752.
(68) Cui, Y.; Wang, Y.; Walter, E. D.; Szanyi, J.; Wang, Y.; Gao, F. Influences of Na+ Co-Cation on the Structure and Performance of Cu/SSZ-13 Selective Catalytic Reduction Catalysts. *Catal. Today* **2020**, *339*, 233–240. https://doi.org/10.1016/j.cattod.2019.02.037.
(69) Gao, F.; Wang, Y.; Washton, N. M.; Kollár, M.; Szanyi, J.; Peden, C. H. F. Effects of Alkali and Alkaline Earth Cocations on the Activity and Hydrothermal Stability of Cu/SSZ-13 NH3–SCR Catalysts. *ACS Catal.* **2015**, *5* (11), 6780–6791. https://doi.org/10.1021/acscatal.5b01621.
(70) Stamatakis, M.; Vlachos, D. G. Unraveling the Complexity of Catalytic Reactions via Kinetic Monte Carlo Simulation: Current Status and Frontiers. *ACS Catal.* **2012**, *2* (12), 2648–2663. https://doi.org/10.1021/cs3005709.
(71) Shih, A. J.; Khurana, I.; Li, H.; González, J.; Kumar, A.; Paolucci, C.; Lardinois, T. M.; Jones, C. B.; Albarracin Caballero, J. D.; Kamasamudram, K.; Yezerets, A.; Delgass, W. N.; Miller, J. T.; Villa, A. L.; Schneider, W. F.; Gounder, R.; Ribeiro, F. H. Spectroscopic and Kinetic Responses of Cu-SSZ-13 to SO2 Exposure and Implications for NOx Selective Catalytic Reduction. *Appl. Catal. Gen.* **2019**, *574*, 122–131. https://doi.org/10.1016/j.apcata.2019.01.024.
(72) Kropf, A. J.; Katsoudas, J.; Chattopadhyay, S.; Shibata, T.; Lang, E. A.; Zyryanov, V. N.; Ravel, B.; McIvor, K.; Kemner, K. M.; Scheckel, K. G.; Bare, S. R.; Terry, J.; Kelly, S. D.; Bunker, B. A.; Segre, C. U. The New MRCAT (Sector 10) Bending Magnet Beamline at the Advanced Photon Source. *AIP Conf. Proc.* **2010**, *1234* (1), 299–302. https://doi.org/10.1063/1.3463194.
(73) Ravel, B.; Newville, M. It ATHENA, It ARTEMIS, It HEPHAESTUS: Data Analysis for X-Ray Absorption Spectroscopy Using It IFEFFIT. *J. Synchrotron Radiat.* **2005**, *12* (4), 537–541. https://doi.org/10.1107/S0909049505012719.
(74) Paolucci, C.; Verma, A. A.; Bates, S. A.; Kispersky, V. F.; Miller, J. T.; Gounder, R.; Delgass, W. N.; Ribeiro, F. H.; Schneider, W. F. Isolation of the Copper Redox Steps in the Standard Selective Catalytic Reduction on Cu-SSZ-13. *Angew. Chem. Int. Ed.* **2014**, *53* (44), 11828–11833. https://doi.org/10.1002/anie.201407030.
(75) Kispersky, V. F.; Kropf, A. J.; Ribeiro, F. H.; Miller, J. T. Low Absorption Vitreous Carbon Reactors for OperandoXAS: A Case Study on Cu/Zeolites for Selective Catalytic Reduction of NOx by NH3. *Phys. Chem. Chem. Phys.* **2012**, *14* (7), 2229–2238. https://doi.org/10.1039/C1CP22992C.
(76) Millan, R.; Cnudde, P.; Hoffman, A. E. J.; Lopes, C. W.; Concepción, P.; van Speybroeck, V.; Boronat, M. Theoretical and Spectroscopic Evidence of the Dynamic Nature of Copper Active Sites in Cu-CHA Catalysts under Selective Catalytic Reduction (NH3–SCR–NOx) Conditions. *J. Phys. Chem. Lett.* **2020**, 10060–10066. https://doi.org/10.1021/acs.jpclett.0c03020.